
JOURNAL OF
ALLOYS AND
COMPOUNDS
materialstoday

ScienceDirect

Journal of Alloys and Compounds

Supports *open access*

7.6 CiteScore

4.65 Impact Factor

About the journal

Editor-in-Chief

Ludwig Schultz
Dresden University of Technology Institute for Materials Science, Germany

Senior Editors

Livio Battezzati
University of Turin Department of Chemistry, Torino, Italy
Thermodynamics of alloys, phase transformations in alloys, solidification, non-equilibrium processing, metallic glasses, metastable compounds, quasicrystals, high temperature alloys, high entropy alloys, nanoporous metals by alloy corrosion. metal oxidation.

Jurgen Buschow
University of Amsterdam Van der Waals-Zeeman Institute, Amsterdam, Netherlands
Solid State Physics; Magnetism; Physical Metallurgy;

Hongge Pan
Zhejiang University School of Materials Science and Engineering, Hangzhou, China
Hydrogen storage materials and hydrides, Anode and cathode materials for rechargeable batteries, Supercapacitor, Magnetic materials, Photocatalystic materials

Vitalij Pecharsky

Iowa State University Department of Materials Science and Engineering, Ames, Iowa, United States
Structure-property relationships; Intermetallic and rare earth compounds. Electronic, magnetic and caloric materials. Mechanochemistry.

Editors

Eiji Abe
The University of Tokyo Graduate School of Engineering Faculty of Engineering Department of Materials Engineering, 7-3-1, Hongo, Bunkyo-ku, 113-865, Bunkyo-Ku, Japan
Microstructures of alloys, Phase transformations in alloys, Electron microscopy (TEM/STEM), X-ray/electron diffraction, Crystallography of alloys/inorganic compounds

Mehmet Acet
University of Duisburg-Essen Faculty of Physics, Duisburg, Germany
Phenomena involving the interplay between magnetism and structure: magnetovolume effects (invar, anti-invar), magnetostructural transitions (Heuslers, anti-perovskites, manganites, and crystallographic properties at interfaces separating different magnetic configurations (shell-ferromagnets); functionalities relevant to refrigeration, energy-conversion, non-volatile magnetic memory, permanent magnets.

Jennifer Aitken
Duquesne University Department of Chemistry and Biochemistry, 600 Forbes Avenue, 308 Mellon Hall, Pittsburgh, Pennsylvania, 15282, United States
Solid-state chemistry, flux synthesis, chalcogenides, nonlinear optical materials, thermoelectrics, single crystal X-ray diffraction, powder X-ray diffraction, semiconductors

Na Chen
Tsinghua University School of Materials Science and Engineering, 100084, Beijing, China
Metallic glasses; Bulk metallic glasses; Glass nanocomposites; Thermodynamics of alloys; Non-equilibrium processing; High entropy alloys; Magnetic thin films

Yuan Chen
The University of Sydney, Sydney, 2006, New South Wales, Australia

Lawrence Cook
Catholic University of America Department of Materials Science and Engineering, 620 Michigan Ave., Washington, District of Columbia, 20064, United States
High temperature materials, Mechanical properties, Phase equilibria, Thermal analysis

Solid-state phase transformations: thermodynamic and kinetic analyses; rapid solidification; metal-activated sintering and Microstructural control in ni(co)-based superalloys, heat-resistance steels, superconducting materials, lead-free solders and ti-al intermetallic compounds.

Nicoleta Lupu
National Institute of Research and Development for Technical Physics, Mangeron Av 47, 6600, Iaşi, Romania
Metallic glasses; Bulk metallic glasses; Magnetic and magnetoelectric materials; Magnetoelastic processes; sensors and devices; Physics and chemistry of surfaces and interfaces; Nanoparticles and nanowire arrays; Hydrogen storage materials.

Valmor Mastelaro
University of Sao Paulo Campus of Sao Carlos, Sao Carlos, Brazil
Structure-property relationships, ZnO Based Materials, Metal Oxide Gas sensors, Glass and Glass-Ceramics, Metal oxide thin films, XAS and XPS spectroscopies

BS Murty
Indian Institute of Technology Hyderabad, IITH Main Road, Near NH-65, Sangareddy, 502285, Kandi, India
Physical metallurgy, alloy design, Phase transformations, High entropy alloys, bulk metallic glasses, nanocrystalline materials, metal matrix composites, electron microscopy, atom probe tomography.

Hari Srikanth
University of South Florida Department of Physics, 4202 E Fowler Ave, Tampa, Florida, FL 33620, United States
Magnetism and magnetic materials, Nanostructured materials for energy and biomedical applications, Structure-property correlations in functional materials, Strongly correlated systems

Wieslaw Strek
Institute of Low Temperature and Structure Research Polish Academy of Sciences, Okólna str. 2, 50-422, Wroclaw, Poland
Rare earth ions and transition metal ions, doped sol-gel materials, photonic structures, nanomaterials, nanoceramics and crystals.

Isabel Van Driessche
Ghent University Department of Chemistry, Krijgslaan 281 (Building S3), 9000, Gent, Belgium
Chemical Solution deposition (CSD, ink jet printing) of ceramics. Materials of interest : superconducting perovskites and buffer layers for production of coated conductors, titanates for (photo)catalytic and battery applications, low-E coatings; Formulation of environmentally friendly based inks. Use of bottom-up chemical synthesis approaches (hydrothermal, microwave-assisted, hot injection) for the synthesis of ceramic nanoparticles/suspensions.

Mingzhong Wu
Colorado State University Department of Physics, 1875 Campus Delivery, Fort Collins, Colorado, CO 80523, United States
Experimental Condensed Matter: Magnetism, Magnetic Materials, Spintronics, and Spin Caloritronics

Renbing Wu
Fudan University Department of Material Science, 200433, Shanghai, China
Semiconductor, Transition Metal-based composites, Electrode materials for energy storage and conversion

Xuezhang Xiao
Zhejiang University School of Materials Science and Engineering, 38 Zheda Road, Hangzhou, China

Volodymyr Yartys
Institute for Energy Technology, 2027, Kjeller, Norway
Nanomaterials for energy storage. Rechargeable Batteries. Hydrogen as an Energy Carrier. New Intermetallics and Carbon Materials for Hydrogen Storage and Battery Applications. Synchrotron and neutron powder diffraction. Crystal structures of novel materials.

Editorial Advisory Board

G. Adachi
Osaka, Japan
Chemistry and materials science of rare earths, Solid state electrochemistry

A.V. Andreev
Praha, Czech Republic
Magnetism of rare-earth and uranium intermetallics, Crystal structure of rare-earth and uranium intermetallics, Metallic hydrides, Permanent magnets

A. Dahle
Jonkoping, Sweden
Solidification, Rheology, Light alloys, Lead-free soldering, Hydrogen storage

F.J. Di Salvo
Ithaca, New York, United States
Synthesis and characterization of solid state compounds, novel crystal structures. Physical properties such as electrical resistivity, thermal conductivity, thermopower.

T.B. Flanagan
Burlington, Vermont, United States
Hydrogen diffusion through metals and alloys, Thermodynamics of H metal systems, Characterization of intermetallic-H systems

C. Gomez Polo
Pamplona, Spain
Magnetism; magnetic nanoparticles and nanostructured magnetic materials; transition metal oxides

J.-M. Greneche
Le Mans, France

V.G. Harris
Boston, Massachusetts, United States
Magnetoceramics, principally ferrites, rf materials, magnetism

Hsiang Hsing-I, PhD
National Cheng Kung University College of Engineering, Tainan, Taiwan
Ceramic processing, Electroceramics, CIGS/CZTS, Powder synthesis

D.C. Johnson
Eugene, Oregon, United States
Solid state chemistry, Thermoelectric materials, X-ray reflectivity, Thermal conductivity, Electrical transport

H. Kleinke
Waterloo, Ontario, Canada
Solid state chemistry, materials chemistry, energy conversion, thermoelectric materials, transport properties, electronic structure calculations, crystal structures, chalcogenides, pnictides

E.J. Mittermeijer
Stuttgart, Germany
Phase transformations, (interface) thermodynamics and kinetics; Nanomaterials, their unusual properties; Stress and phase transformations in (very) thin (multi)layers; surface engineering (nitriding and nitrocarburizing of iron, iron alloys and steels); oxidation of metals and alloys

Y. Mozharivskyj
Hamilton, Ontario, Canada
Thermoelectric materials, Magnetocaloric materials, X-ray analysis

R. Nesper
Zurich, Switzerland
Inorganic chemistry, Zintl phases, nanoscience, intermetallic phases, electrochemistry, hard materials.

E. Peterson
Los Alamos, New Mexico, United States
Actinide thermodynamics and equilibrium phase diagrams, High temperature superconductor synthesis, characterization, and applications, Carbon nanotubes, Radiation damage, and Vaporization studies

W. Prellier
Caen, France

K. Z. Rožman
Ljubljana, Slovenia

H. Sakaguchi
Tottori, Japan
Li ion materials, Hydrogen storage materials, hydrides

H. Sato
Tokyo, Japan

O.N. Senkov
Dayton, Ohio, United States

K. Suzuki
Miyagi, Japan

T. Takabatake
Higashihiroshima, Japan

T. Yamase
Yokohama, Japan
Catalysis, photoluminescence.

C.-L. Yeh
Taichung, Taiwan
Self-propagating High-temperature Synthesis (SHS), Transition metal borides and nitrides, Intermetallics, MAX phases, Thermite Reaction

All members of the Editorial Board have identified their affiliated institutions or organizations, along with the corresponding country or geographic region. Elsevier remains neutral with regard to any jurisdictional claims.

ISSN: 0925-8388

Journal of Alloys and Compounds

Supports *open access*

7.6

CiteScore

Volume 820

15 April 2020

Previous vol/issue Next vol/issue

Journal of Alloys and Compounds
Supports *open access*

7.6
CiteScore

Purchase PDF Article preview

Research article ○ Abstract only

Phase dependent selectivity shifting behavior of Cd_2SnO_4 nanoparticles based gas sensor towards volatile organic compounds (VOC) at low operating temperature

Deshraj Meena, Bharti Singh, Abhishek Anand, Mukhtiyar Singh, M.C. Bhatnagar

Article 153117

Purchase PDF Article preview

Research article ○ Abstract only

First-principles calculations of a new half-metallic Heusler alloy FeCrAs

ZhaoPeng Hao, Ran Liu, YiHang Fan, LiLi Wang

Article 153118

Purchase PDF Article preview

Research article ○ Abstract only

Strong metallic glass: TiZrHfCuNiBe high entropy alloy

Y. Tong, J.C. Qiao, J.M. Pelletier, Y. Yao

Article 153119

Purchase PDF Article preview

Research article ○ Abstract only

Controllable synthesis of reduced graphene oxide/nickel hydroxide composites with different morphologies for high performance supercapacitors

Liuqin Lai, Rong Li, Siyu Su, Liang Zhang, ... Xiaohong Zhu

Article 153120

Purchase PDF Article preview

Research article ○ Abstract only

A study for pre-processing of Nb diffusion in Nb–N layer by double-glow plasma alloying

Jinwei Yi, Qiang Miao, Wenping Liang, Zheng Ding, ... Yang Li

Article 153121

Purchase PDF Article preview

Research article ○ Abstract only

Grain refinement mechanism and improved mechanical properties in Mg–Sn alloy with trace Y addition

X.Y. Qian, Y. Zeng, B. Jiang, Q.R. Yang, ... F.S. Pan

Article 153122

Purchase PDF Article preview

Journal of Alloys and Compounds
Supports *open access*

7.6
CiteScore

Fangfang Li, Lei Lu, Xiandong Meng, Hong Xiao, ... Peng Shi
Article 153124

Purchase PDF Article preview

Research article ○ Abstract only

Unveiling the relationships between (010) facets-orientation growth and photocatalytic activity in $W_{18}O_{49}$ nanowires
Guojuan Hai, Jianfeng Huang, Yanni Jie, Liyun Cao, ... Liangliang Feng
Article 153127

Purchase PDF Article preview

Research article ○ Abstract only

TiO_2 nanotube array modified with polypyrrole for efficient photoelectrocatalytic decolorization of methylene blue
Jialin Zhang, Zengyuan Pang, Qian Sun, Xin Chen, ... Ioannis S. Chronakis
Article 153128

Purchase PDF Article preview

Research article ○ Abstract only

Structural and chemical mechanism underlying formation of Zn_2SiO_4:Mn crystalline phosphor properties
Tatiana I. Krasnenko, Andrei N. Enyashin, Natalia A. Zaitseva, Rina F. Samigullina, ... Tatiana A. Onufrieva
Article 153129

Purchase PDF Article preview

Research article ○ Abstract only

Room-temperature magnetoelectric effect in Al-doped $Sr_3Co_2(Fe_{1-x}Al_x)_{24}O_{41}$ hexaferrites
Chongsheng Wu, Yingli Liu, Qian Liu, Yu Wang, ... Huaiwu Zhang
Article 153130

Purchase PDF Article preview

Research article ○ Abstract only

Effect of heat treatment on erosion–corrosion of Fe-based amorphous alloy coating under slurry impingement
Fei Huang, Jia-jie Kang, Wen Yue, Xiao-bin Liu, ... Cheng-biao Wang
Article 153132

Purchase PDF Article preview

Research article ○ Abstract only

Hydrothermal synthesis of In_2O_3 nanocubes for highly responsive and selective ethanol gas sensing
Thuy T.D. Nguyen, Ha-Nui Choi, M. Jamir Ahemad, Dung Van Dao, ... Yeon-Tae Yu
Article 153133

Purchase PDF Article preview

Journal of Alloys and Compounds
Supports *open access*

7.6
CiteScore

DanDan Wang, WuBian Tian, JianXiang Ding, YongFa Zhu, ... ZhengMing Sun
Article 153136

Purchase PDF Article preview

Research article ○ Abstract only

Effect of high hardness and adhesion of gradient TiAlSiN coating on cutting performance of titanium alloy
Wenzhang Lü, Guojian Li, Yaoyao Zhou, Shiying Liu, ... Qiang Wang
Article 153137

Purchase PDF Article preview

Research article ○ Abstract only

Magnetocaloric effect and sign reversal of magnetic entropy change across the spin reorientation temperature in $R_3Fe_5O_{12}$ (R = Gd, Dy)
Canglong Li, Godfrey Okumu Barasa, Yang Qiu, Songliu Yuan
Article 153138

Purchase PDF Article preview

Research article ○ Abstract only

Delicate manipulation of cobalt oxide nanodot clusterization on binder-free TiO_2-nanorod photoanodes for efficient photoelectrochemical catalysis
Han Feng, Liangliang Liang, Junyu Ge, Weiyi Wu, ... Lin Li
Article 153139

Purchase PDF Article preview

Research article ○ Abstract only

Synergism of Cu and Al co-doping on improvements of structural integrity and electrochemical performance for $LiNi_{0.5}Mn_{1.5}O_4$
Shiyou Li, Yuan Wei, Peng Wang, Yaohua Feng, ... Xiaoling Cui
Article 153140

Purchase PDF Article preview

Research article ○ Abstract only

Micro-mechanical properties of new alternative binders for cemented carbides: $CoCrFeNiW_x$ high-entropy alloys
Xiaoqing Li, Daixiu Wei, Levente Vitos, Raquel Lizárraga
Article 153141

Purchase PDF Article preview

Research article ○ Abstract only

Fabrication of pH-responsive PAA-$NaMnF_3$@DOX hybrid nanostructures for magnetic resonance imaging and drug delivery

Journal of Alloys and Compounds
Supports *open access*

7.6
CiteScore

Purchase PDF Article preview

Research article ○ Abstract only

MoS$_2$ nanosheets/graphitized porous carbon nanofiber composite: A dual-functional host for high-performance lithium–sulfur batteries

Chaoshuai Chai, Hua Tan, Xiaoyan Fan, Kai Huang

Article 153144

Purchase PDF Article preview

Research article ○ Abstract only

Structural and multiferroic properties in double-layer Aurivillius phase $Pb_{0.4}Bi_{2.1}La_{0.5}Nb_{1.7}Mn_{0.3}O_9$ prepared by molten salt method

Tio Putra Wendari, Syukri Arief, Nandang Mufti, Andon Insani, ... Zulhadjri

Article 153145

Purchase PDF Article preview

Research article ○ Abstract only

Growth and characterisation of ZnO micro/nanostructures doped with cerium for photocatalytic degradation applications

M. Rodríguez-Peña, G. Flores-Carrasco, A. Urbieta, M.E. Rabanal, P. Fernández

Article 153146

Purchase PDF Article preview

Research article ○ Abstract only

Construction of uniform SnS_2/ZnS heterostructure nanosheets embedded in graphene for advanced lithium-ion batteries

Canpei Wang, Yingying Zhang, Yongsheng Li, Yan Zhang, ... Jianmin Zhang

Article 153147

Purchase PDF Article preview

Research article ○ Abstract only

The role of Al^{+3} on the microstructural and electrical properties of $Na_{1+x}Al_xTi_{2-x}(PO_4)_3$ NASICON glass-ceramics

Adriana M. Nieto-Muñoz, Jairo F. Ortiz-Mosquera, Ana C.M. Rodrigues

Article 153148

Purchase PDF Article preview

Research article *Open access*

Early stage phase separation of $AlCoCr_{0.75}Cu_{0.5}FeNi$ high-entropy powder at the nanoscale

Nicolas J. Peter, Maria J. Duarte, Christian H. Liebscher, Vikas C. Srivastava, ... Gerhard Dehm

Article 153149

Journal of Alloys and Compounds
Supports *open access*

7.6
CiteScore

Research article ○ Abstract only

Synthesis, structure and optical properties of layered $M_4Nb_6O_{17}\cdot nH_2O$ (M = K, Rb, Cs) hexaniobates

Eduardo Caetano C. Souza

Article 153152

Purchase PDF Article preview

Research article ○ Abstract only

Effect of sintering temperature on the mechanical properties and microstructures of pressureless-sintered B_4C/SiC ceramic composite with carbon additive

Yu Zhu, Dujun Luo, Zongjia Li, Yangwei Wang, ... Tao Chen

Article 153153

Purchase PDF Article preview

Research article ○ Abstract only

Electromagnetic and microwave absorption properties of Ti_3SiC_2 powders decorated with Ag particles

Yi Liu, Chen Ji, Xiaolei Su, Jie Xu, Xinhai He

Article 153154

Purchase PDF Article preview

Research article ○ Abstract only

Study on high temperature deformation behavior of WC-10 wt %Ni_3Al cemented carbide

Minai Zhang, Alexander D. Dupuy, Jingmao Li, Xin Wang, ... Xiaoqiang Li

Article 153156

Purchase PDF Article preview

Research article ○ Abstract only

Facile self-assembling of three-dimensional graphene/solvent free carbon nanotubes fluid framework for high performance supercapacitors

Liang Zhou, Jinyu Wang, Zhikang Liu, Junwei Yang, ... Chuanxi Xiong

Article 153157

Purchase PDF Article preview

Research article ○ Abstract only

Synthesis of Ni–Co–ZrO_2 nanocomposites doped with ceria particles via electrodeposition as highly protective coating

Baosong Li, Weiwei Zhang

Article 153158

Purchase PDF Article preview

Research article ○ Abstract only

Journal of Alloys and Compounds
Supports *open access*

7.6
CiteScore

Kong Eng Ng, Poh Choon Ooi, Muhammad Aniq Shazni Mohammad Haniff, Boon Tong Goh, ... Mohd Ambri Mohamed
Article 153160

Purchase PDF Article preview

Research article ○ Abstract only

Ultrafine trimetallic oxyphosphide nanoparticles for efficient electrochemical overall water splitting
Zhao Li, Guofeng Qiu, Yanchao Shen, Xiang Wang, ... Lin Tian
Article 153161

Purchase PDF Article preview

Research article ○ Abstract only

Emission enhancement of bifunctional $La_2MoO_6:Sm^{3+}$ nanoparticles by doping Y^{3+} ions for flexible display and high CRI WLEDs
Yongbin Hua, Jae Su Yu
Article 153162

Purchase PDF Article preview

Research article ○ Abstract only

Formation, structure and properties of pseudo-high entropy clustered bulk metallic glasses
A. Inoue, F.L. Kong, S.L. Zhu, B.L. Shen, ... W.J. Botta
Article 153164

Purchase PDF Article preview

Research article ○ Abstract only

Long-term room-temperature aging treatment of a bulk metallic glass composite
Peng Xue, Yongjiang Huang, Simon Pauly, Songshan Jiang, ... Jianfei Sun
Article 153165

Purchase PDF Article preview

Research article ○ Abstract only

Switching g-C_3N_4 morphology from double-walled to single-walled microtubes induced high photocatalytic H_2-production performance
Runren Jiang, Guanghua Lu, Ranran Zhou, Haohan Yang, ... Matthew Nkoom
Article 153166

Purchase PDF Article preview

Research article ○ Abstract only

The high-energy milling process as a synergistic approach to minimize the thermal conductivity of PbTe nanostructures
H. Rojas-Chávez, J.M. Juárez-García, R. Herrera-Rivera, E. Flores-Rojas, ... M.L. Mondragón-Sánchez

Journal of Alloys and Compounds
Supports *open access*

7.6
CiteScore

Purchase PDF Article preview

Research article ○ Abstract only

Anomalous photoemission in bismuth-doped amorphous solid via selective reduction and energy transfer mechanism investigation

Weirong Wang, Chun Jiang

Article 153169

Purchase PDF Article preview

Research article ○ Abstract only

Rapid precipitation of intermetallic phases during isothermal treatment of duplex stainless steel joints produced by friction stir welding

Igor J. Marques, Flavio J. Silva, Tiago F.A. Santos

Article 153170

Purchase PDF Article preview

Research article ○ Abstract only

Fabrication and spectral properties of Nd:S-FAP transparent ceramics by simple route of HP method

Yongqiang Zhang, Bingchu Mei, Weiwei Li, Yu Yang, ... Zuodong Liu

Article 153171

Purchase PDF Article preview

Research article ○ Abstract only

N/Ti^{3+} co-doping biphasic TiO_2/Bi_2WO_6 heterojunctions: Hydrothermal fabrication and sonophotocatalytic degradation of organic pollutants

Mingxuan Sun, Yuan Yao, Wen Ding, Sambandam Anandan

Article 153172

Purchase PDF Article preview

Research article ○ Abstract only

Processing and properties of novel $ZnO–Bi_2O_3–B_2O_3$ glass-ceramic nanocomposites

Casey M. Schwarz, Myungkoo Kang, Quentin Altemose, Katrina Raichle, ... Stephen M. Kuebler

Article 153173

Purchase PDF Article preview

Research article ○ Abstract only

Ce and Fe doped gahnite: Cost effective solar reflective pigment for cool coating applications

V. Elakkiya, Shanmugam Sumathi

Article 153174

Journal of Alloys and Compounds
Supports *open access*

7.6
CiteScore

Research article ○ Abstract only

Synthesis, characterization, and properties of two new phosphate crystals $MZnAl(PO_4)_2$ (M = Na, K) with 3D framework tunnel structures

Hao Wang, Lei Geng, Yun-Jian Wang, Hong-Yan Lu, Chang-Yu Meng

Article 153176

Purchase PDF Article preview

Research article ○ Abstract only

Ferroelastic domain switching toughening in Ce–Y–La co-stabilized zirconia ceramics obtained from coated starting powders

Zhaoyubo Zeng, Yunzhong Liu, Yingxiang Zhang, Zhiguang Zhou, Xiaohui Liu

Article 153177

Purchase PDF Article preview

Research article ○ Abstract only

Mechanical tensile strain for AlGaN/GaN metal-insulator-semiconductor high-electron-mobility transistors on a silicon-on-insulator substrate

Hsuan-Ling Kao, Cheng-Lin Cho, Hsien-Chin Chiu, Hou-Yu Wang, ... H.H. Hsu

Article 153178

Purchase PDF Article preview

Research article ○ Abstract only

Effects of transition elements on the site preference, elastic properties and phase stability of $L1_2$ γ′-Co_3(Al, W) from first-principles calculations

Xingjun Liu, Yichun Wang, Wei-Wei Xu, Jiajia Han, Cuiping Wang

Article 153179

Purchase PDF Article preview

Research article ○ Abstract only

Structure and magnetic performance of Gd substituted Sr-based hexaferrites

Jiyu Hu, Chaocheng Liu, Xucai Kan, Xiansong Liu, ... Khalid Mehmood Ur Rehman

Article 153180

Purchase PDF Article preview

Research article ○ Abstract only

High strength and high ductility in a novel $Fe_{40.2}Ni_{11.3}Mn_{30}Al_{7.5}Cr_{11}$ multiphase high entropy alloy

Margaret Wu, Ian Baker

Article 153181

Purchase PDF Article preview

Journal of Alloys and Compounds
Supports *open access*

7.6
CiteScore

precipitant
Nianying Zhou, Shuai Sha, Yin Zhang, Sha Li, ... Jiapan Luan
Article 153183

Purchase PDF Article preview

Research article ○ Abstract only
The mixture of silver nanowires and nanosilver-coated copper micronflakes for electrically conductive adhesives to achieve high electrical conductivity with low percolation threshold
Qian Wang, Shuye Zhang, Guiming Liu, Tiesong Lin, Peng He
Article 153184

Purchase PDF Article preview

Research article ○ Abstract only
Self-supported Hierarchical $Fe(PO_3)_2$@Cu_3P nanotube arrays for efficient hydrogen evolution in alkaline media
Dongmei Dai, Bo Wei, Ying Li, Xiao Ma, ... Lingling Xu
Article 153185

Purchase PDF Article preview

Research article ○ Abstract only
Facile green synthesis and characterization of *Crataegus microphylla* extract-capped silver nanoparticles (CME@Ag-NPs) and its potential antibacterial and anticancer activities against AGS and MCF-7 human cancer cells
Sobhan Mortazavi-Derazkola, Mohammad Ali Ebrahimzadeh, Omid Amiri, Hamid Reza Goli, ... Masoud Salavati-Niasari
Article 153186

Purchase PDF Article preview

Research article ○ Abstract only
Enhanced hydrogen absorption kinetics by introducing fine eutectic and long-period stacking ordered structure in ternary eutectic Mg–Ni–Y alloy
Wenjie Song, Huiping Dong, Guang Zhang, Jie Liu, ... Qiuming Wei
Article 153187

Purchase PDF Article preview

Research article ○ Abstract only
Improved optoelectronic properties of Gd doped cadmium oxide thin films through optimized film thickness for alternative TCO applications
P. Sakthivel, S. Asaithambi, M. Karuppaiah, R. Yuvakkumar, ... G. Ravi
Article 153188

Purchase PDF Article preview

Journal of Alloys and Compounds
Supports *open access*

7.6
CiteScore

micro-nanocrystals
Mimi Li, Youkui Xu, Guoqiang Peng, Jintao Liu, ... Zhipeng Ci
Article 153190

Purchase PDF Article preview

Research article ○ Abstract only

A highly selective and sensitive fluorescent probe for detecting Cr(VI) and cell imaging based on nitrogen-doped graphene quantum dots
Liying Sheng, Baihe Huangfu, Qinhai Xu, Wenli Tian, ... Shuqin Tan
Article 153191

Purchase PDF Article preview

Research article ○ Abstract only

Lattice vibration properties of $MoS_2/PtSe_2$ heterostructures
Kuilong Li, Tianyi Wang, Wenjia Wang, Xingguo Gao
Article 153192

Purchase PDF Article preview

Review article ○ Abstract only

A review on WO_3 based gas sensors: Morphology control and enhanced sensing properties
Chengjun Dong, Rongjun Zhao, Lijia Yao, Yan Ran, ... Yude Wang
Article 153194

Purchase PDF Article preview

ISSN: 0925-8388

Journal of Alloys and Compounds 820 (2020) 153145

Contents lists available at ScienceDirect

Journal of Alloys and Compounds

journal homepage: http://www.elsevier.com/locate/jalcom

Structural and multiferroic properties in double-layer Aurivillius phase $Pb_{0.4}Bi_{2.1}La_{0.5}Nb_{1.7}Mn_{0.3}O_9$ prepared by molten salt method

Tio Putra Wendari [a], Syukri Arief [a], Nandang Mufti [b], Andon Insani [c], Jacob Baas [d], Graeme R. Blake [d], Zulhadjri [a, *]

[a] Department of Chemistry, Faculty of Mathematics and Natural Sciences, Universitas Andalas, Kampus Limau Manis, Padang, 25163, Indonesia
[b] Department of Physics, Faculty of Mathematics and Natural Sciences, Universitas Negeri Malang, Jl. Semarang 5, Malang, 65145, Indonesia
[c] Center for Science and Technology of Advanced Materials, National Nuclear Energy Agency of Indonesia, Puspiptek Serpong, Tangerang Selatan, 15314, Indonesia
[d] Zernike Institute for Advanced Materials, University of Groningen, Nijenborgh 4, 9747, AG Groningen, the Netherlands

ARTICLE INFO

Article history:
Received 14 August 2019
Received in revised form
26 October 2019
Accepted 22 November 2019
Available online 22 November 2019

Keywords:
Double-layer Aurivillius phase
Molten salt method
Cation disorder
Multiferroic
Relaxor-ferroelectric behavior
Ferromagnetic interactions

ABSTRACT

A single-phase sample of the Aurivillius compound $Pb_{0.4}Bi_{2.1}La_{0.5}Nb_{1.7}Mn_{0.3}O_9$ was prepared by a molten salt method using K_2SO_4/Na_2SO_4 as the flux. The crystal structure, morphology, ferroelectric, and magnetic properties were investigated. Neutron powder diffraction data confirmed a non-centrosymmetric orthorhombic crystal structure with space group $A2_1am$ and Pb/Bi disorder in the bismuth oxide blocks, Bi/Pb/La disorder on the perovskite *A*-site, and Nb/Mn disorder on the perovskite *B*-site. The morphology of the sample showed anisotropic plate-like grains as probed by scanning electron microscopy. The dielectric constant exhibits a transition peak between 600 K and 640 K that depends on frequency, indicating relaxor ferroelectric behavior. Electrical polarization versus applied field loops are unsaturated, with a remnant polarization of 0.43 $\mu C/cm^2$ at 40 Hz under the maximum electrical field applied of 160 kV/cm. The ferroelectricity originates from the displacement of oxygen atoms in the BO_6 octahedra, resulting in a polar structural distortion. Magnetic susceptibility measurements showed the presence of mixed Mn^{3+} and Mn^{4+}, resulting in short-range ferromagnetic order via double exchange interactions below 33 K. The remnant magnetization (M_r) is 0.01 emu/g at 5 K. This mixed valence of Mn cations is mainly responsible for the high electrical conductivity. Thus, $Pb_{0.4}Bi_{2.1}La_{0.5}Nb_{1.7}Mn_{0.3}O_9$ exhibits coexisting ferroelectric and ferromagnetic properties.

1. Introduction

Multiferroic compounds presenting the coexistence of ferroelectric and ferromagnetic order have attracted a lot of attention for several decades due to their interesting properties and potential applications for data storage devices (RAM), sensors, spintronic and other electronic devices [1–3]. Among them, the Aurivillius compounds are of particular interest due to their structural flexibility. The Aurivillius structure is constructed from alternating perovskite-like blocks and bismuth oxide blocks and can be represented by the general formula $(Bi_2O_2)^{2+}(A_{m-1}B_mO_{3m+1})^{2}$, where *A* is a mono-, di-, or trivalent cation with dodecahedral coordination, *B* is a transition metal cation with octahedral coordination, and *m* is the number of octahedral layers within the perovskite-like blocks [4]. This structure can accommodate a wide range of *A*- and *B-site* cation substitutions, allowing control of the physical properties.

Lead and bismuth-based Aurivillius compounds have drawn particular attention due to their favorable electrical properties and high ferroelectric Curie temperatures, with potential use in random access memory (RAM) [5]. The effect of the $6s^2$ lone pair of Pb^{2+} and Bi^{3+} induces cation shifts that break inversion symmetry, which can result in ferroelectricity in these compounds [6–8]. However, few Aurivillius phases exhibit both ferroelectric and ferromagnetic properties due to the contradictory character of the *B*-cation which is generally d^0 in ferroelectric compounds and d^n ($n \neq 0$) in magnetic compounds [9]. Therefore, studies with the aim of improving the properties of Aurivillius compounds have been focused in recent years especially on inducing the coexistence of both ferroelectric and ferromagnetic properties.

The introduction of first-row transition metal cations with a

* Corresponding author.
E-mail address: zulhadjri@sci.unand.ac.id (Zulhadjri).

https://doi.org/10.1016/j.jallcom.2019.153145
0925-8388/

partially filled *d*-shell (d^n) on the perovskite *B*-site can potentially give rise to multiferroic properties in Aurivillius phases. It is well known that $BiMnO_3$ exhibits coupling between ferroelectricity and ferromagnetism [1,10,11]. Since it is believed that the ferroelectricity of perovskite-based compounds arises mainly from the distortion of BO_6 octahedra, the partial substitution of Mn^{3+} (d^4) for Nb^{5+} (d^0) on the Aurivillius *B*-site might improve the ferroelectric properties due to the effect of different ionic radii, as well as introducing a magnetic moment [12–14]. The substitution of Ln^{3+} cations on the Aurivillius *A*-site has previously been shown to improve the dielectric and ferroelectric properties [15,16].

Recently, we have reported on the novel series of compounds $Pb_{1-2x}Bi_{1.5+2x}La_{0.5}Nb_{2-x}Mn_xO_9$ synthesized by the molten salt method, for which single-phase products can be obtained for the compositions $0 \leq x \leq 0.3$ [17]. These compounds adopt a non-centrosymmetric crystal structure and cation disorder is found in both the bismuth oxide and perovskite blocks by Raman analysis, leading to greater structural distortion. The sample of $Pb_{0.4}Bi_{2.1}La_{0.5}Nb_{1.7}Mn_{0.3}O_9$ with maximum Mn content exhibits the most distorted structure of the series and is expected to give the most pronounced magnetic properties.

Herein, we present a further structural investigation using neutron powder diffraction to study the atomic-scale disorder and the structural distortion that would favor enhanced ferroelectricity. The ferroelectric and magnetic properties of this compound are also investigated in detail to demonstrate the multiferroic properties.

2. Experimental procedure

Single-phase $Pb_{0.4}Bi_{2.1}La_{0.5}Nb_{1.7}Mn_{0.3}O_9$ was synthesized using a molten-salt method as reported in Ref. [17]. Neutron powder diffraction (NPD) data were collected on the High Resolution Powder Diffractometer (DN3) at the Section for Neutron Beam Technology of the Center for Science and Technology of Advanced Materials (BATAN), Indonesia. The wavelength of the incident neutron beam was 1.8195 Å and data were collected for 11 h at room temperature. The structural parameters were refined by the Rietveld technique using the RIETICA program [18]. For electrical measurements, the powder was pressed into pellets and sintered at 1173 K for 5 h. Silver conductive paste (Aldrich, 99%) was applied to both surfaces of the sintered pellet as the electrodes and heated at 423 K for 2 h. Capacitance was measured as a function of temperature using a precision LCR-meter (Agilent 4980A) with an amplitude of 1 V at different frequencies up to 1 MHz. Room temperature ferroelectric hysteresis was measured using a ferroelectric tester (TF analyzer, AixACCT) at 40 Hz. Magnetic susceptibility was measured using a SQUID magnetometer (Quantum Design MPMS XL7) in the temperature range from 5 to 300 K under applied magnetic fields of 1 T and 100 Oe. Magnetization as a function of applied field was measured from −5 T to 5 T at temperatures of 5 K and 150 K.

3. Results and discussion

$Pb_{0.4}Bi_{2.1}La_{0.5}Nb_{1.7}Mn_{0.3}O_9$ has an orthorhombic structure with the $A2_1am$ space group as previously reported using XRD analysis [17]. Detailed structural parameters were obtained from Rietveld refinement of the NPD data. The initial structural model used was that of the parent compound $PbBi_2Nb_2O_9$ with the $A2_1am$ space group [19]. Here all atoms occupy general Wyckoff positions 8*b* except for Bi(1) and O(1) in the perovskite block which occupy 4*a* positions. It is well established that cations with lone pair electrons prefer to occupy the Bi-site in the bismuth oxide blocks, which suggests that Pb^{2+} may substitute in this block [8,20]. Disorder between Mn and Nb is likely in the BO_6 octahedra. The perovskite *A*-site can be occupied by Pb, Bi and La.

Since the absence of an active lone pair of electrons limits the probability that La^{3+} occupies the Bi-site of the bismuth oxide blocks, which was also suggested by Raman spectroscopy as reported previously [17], we performed the initial refinement with a 50% occupancy of La^{3+} on the Pb(1) site in the perovskite block. The site occupancies of Pb(1)/Bi(1), Pb(2)/Bi(2) and Nb(1)/Mn(1) were then adjusted manually to optimize the fit while the atomic positions were refined automatically. Fig. 1 shows the Rietveld fits to the NPD data and the refined parameters are summarized in Table 1. The Bi(2) sites in the bismuth oxide blocks are occupied by a random distribution of Pb^{2+} (12.5%) and Bi^{3+} (87.5%). Kennedy et al. [21] observed a similar preference of Pb^{2+} for the bismuth oxide blocks in $Pb_{1-x}Sr_xBi_2Nb_2O_9$, even for low-Pb compositions. In the perovskite blocks of our current material, the Pb(1) *A*-site is occupied by 50% La^{3+}, 35% Bi^{3+}, and 15% Pb^{2+}. This preference for a disordered distribution of Pb^{2+} and Bi^{3+} in both the bismuth oxide blocks and the perovskite *A*-site is also in agreement with earlier reports and is consistent with the similar electronic structures of the two cations [8,20]. According to the nominal formula of $Pb_{0.4}Bi_{2.1}La_{0.5}Nb_{1.7}Mn_{0.3}O_9$, the perovskite *B*-site should be occupied by Nb^{5+} and Mn^{3+} cations with fractions of 85% and 15%, respectively. Thus, the formula is perhaps more usefully written as $(Bi_{1.75}Pb_{0.25})O_2(Pb_{0.15}Bi_{0.35}La_{0.5}Nb_{1.7}Mn_{0.3})O_7$ in order to reflect the occupation of each cation in the bismuth and perovskite blocks. A representation of the crystal structure is shown in Fig. 2.

Since it is believed that the off-center distortion of the *B*-site cation is responsible for ferroelectricity in Aurivillius compounds, we focus on atomic displacements associated with the BO_6 octahedra. The *B*(1) cation is displaced from the center of the octahedra along the *c*-axis resulting in longer *B*(1)–O(1) and shorter *B*(1)–O(2) bond distances as summarized in Table 2 (see also Fig. 2(c)). The *B*-site cations are also shifted along the *a* and *b* axes, evidenced by the different *B*(1)–O(4) and *B*(1)–O(5) distances. Displacement of the oxygen atoms from their ideal positions also results in tilting

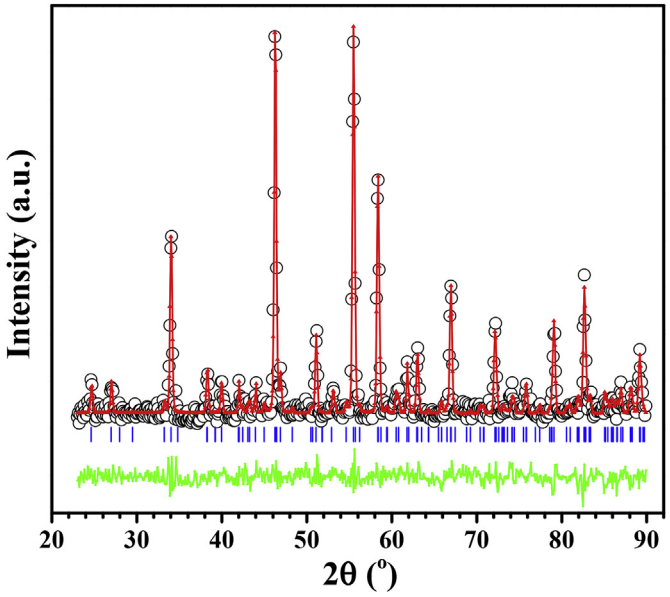

Fig. 1. Rietveld fits to NPD data for single-phase $Pb_{0.4}Bi_{2.1}La_{0.5}Nb_{1.7}Mn_{0.3}O_9$: experimental data (black circles), calculated profile (red line), and difference profile (green line). The blue tick marks indicate the positions of allowed Bragg reflections in the space group $A2_1am$. (For interpretation of the references to colour in this figure legend, the reader is referred to the Web version of this article.)

Table 1
Refined structural parameters for $Pb_{0.4}Bi_{2.1}La_{0.5}Nb_{1.7}Mn_{0.3}O_9$ from NPD data at room temperature using the orthorhombic space group $A2_1am$, with $Z = 4$.

Atom	Site	x	y	z	Occ. (n)
Pb(1)	4*a*	0	0.2467(7)	0	0.15
Bi(1)	4*a*	0	0.2467(7)	0	0.35
La(1)	4*a*	0	0.2467(7)	0	0.5
Bi(2)	8*b*	0.4993(1)	0.7377(3)	0.2011(4)	0.875
Pb(2)	8*b*	0.4993(1)	0.7377(3)	0.2011(4)	0.125
Nb(1)	8*b*	0.4641(2)	0.7289(7)	0.4134(6)	0.850
Mn(1)	8*b*	0.4641(2)	0.7289(7)	0.4134(6)	0.150
O(1)	4*a*	0.4561(4)	0.1947(1)	0	1.0
O(2)	8*b*	0.4791(6)	0.7787(8)	0.3386(2)	1.0
O(3)	8*b*	0.7213(1)	0.0141(6)	0.25	1.0
O(4)	8*b*	0.7035(2)	0.9561(2)	0.0774(1)	1.0
O(5)	8*b*	0.7474(4)	0.9877(7)	0.5690(1)	1.0

$a = 5.4910(5)$ Å, $b = 5.4874(3)$ Å, $c = 25.1229(7)$ Å; $V = 757.0007(9)$ Å^3.
$R_p = 14.04\%$, $R_{bragg} = 3.48$, $\chi^2 = 1.504$.

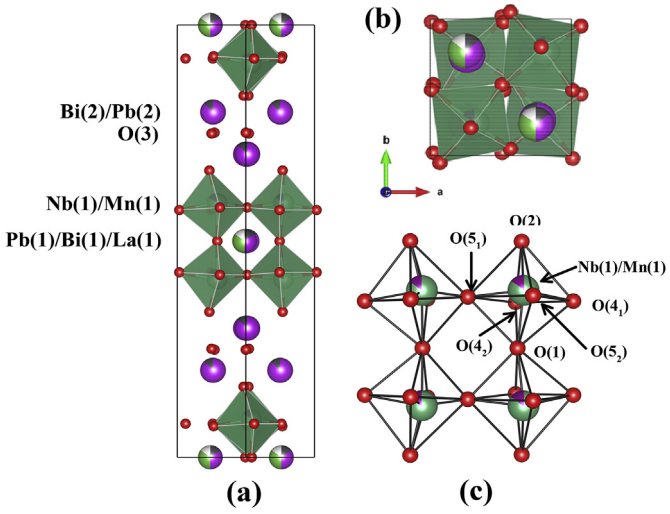

Fig. 2. **(a)** Orthorhombic structure of $Pb_{0.4}Bi_{2.1}La_{0.5}Nb_{1.7}Mn_{0.3}O_9$ (*ac*-plane view). **(b)** Distortion of perovskite blocks projected in the *ab* plane. **(c)** View of linked BO_6 octahedra.

Table 2
Interatomic bond distances and bond angles associated with the BO_6 octahedra (B = Nb or Mn).

Bond	Bond distance (Å)	Bond	Bond Angle (°)
B(1)–O(1)	2.1842(2)	O(2)-B(1)-O(1)	176.39
B(1)–O(2)	1.8996(2)	O(4)- B(1)-O(5)	159.42
B(1)–O(4$_1$)	1.7695(0)	B(1)-O(1)- B(1)	169.88
B(1)–O(4$_2$)	2.0056(4)	B(1)-O(5)- B(1)	153.46
B(1)–O(5$_1$)	2.0072(1)		
B(1)–O(5$_2$)	2.1525(2)		

of the BO_6 octahedra, as clearly seen in Fig. 2(b). This tilting leads to a more distorted crystal structure and results in a difference between the *a* and *b* lattice parameters. The degree of octahedral distortion can be quantified by the orthorhombicity ratio $(a-b)/(a+b)$ of 0.00033 [9]. This distortion is driven both by cation disorder and size mismatch between the perovskite *A*- and *B*-sites and further contributes to the ferroelectric displacement.

The morphology and size of the sample grains was previously investigated using SEM in Ref. [17]. The grains are highly anisotropic and plate-like, which is a typical feature of Aurivillius phases. The average grain size is in the range 2.7–3.1 μm.

The frequency dependence of the dielectric constant and

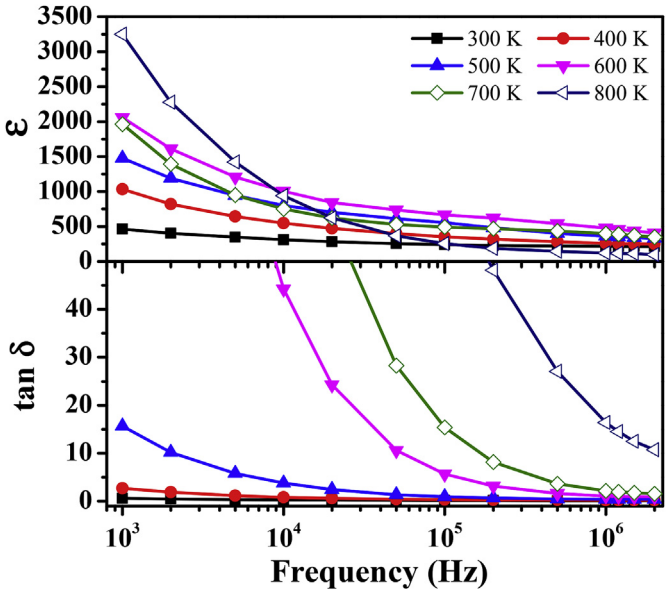

Fig. 3. Frequency dependence of dielectric constant (ϵ) and loss (tan δ) of $Pb_{0.4}Bi_{2.1}La_{0.5}Nb_{1.7}Mn_{0.3}O_9$ at different temperatures.

dielectric loss of $Pb_{0.4}Bi_{2.1}La_{0.5}Nb_{1.7}Mn_{0.3}O_9$ at different temperatures is shown in Fig. 3. It is observed that the dielectric constant decreases as frequency increases and becomes stable at frequencies above 10 kHz, which is consistent with the behavior of ordinary ferroelectric materials. The higher dielectric constant at lower frequencies is due to the contribution of different polarizations (i.e. dipolar, ionic, electronic, and interfacial) [22]. This behavior is also caused by the accumulation of charge carriers on the surface and at grain boundaries, explained by the Maxwell-Wagner effect [12]. Thus, high values of the dielectric constant at low frequencies are not only caused by intrinsic but also by extrinsic factors. It is also clearly seen in Fig. 3 that the dielectric constant initially increases with temperature and then significantly decreases from 600 K to 700 K, suggesting that the sample has a ferroelectric-paraelectric transition (T_c) in this temperature range. The dielectric loss increases slightly with temperature below 600 K, and then more rapidly at higher temperature, which can also indicate a transition to the paraelectric phase where the sample becomes more conducting. Moreover, at high temperature, the electrical conductivity is enhanced by thermal effects as is the case for most semiconductors, resulting in a significant increase of the dielectric loss [23].

Fig. 4 shows the temperature dependence of the dielectric constant (ϵ) and dielectric loss (tan δ) at high frequencies, which best reflect the intrinsic polarizability. A single peak in the dielectric constant is observed between 600 K and 640 K depending on frequency, corresponding to T_c. Compared with the parent compound $PbBi_2Nb_2O_9$ for which $T_c = 830$ K [24], the transition temperature is significantly decreased for $Pb_{0.4}Bi_{2.1}La_{0.5}Nb_{1.7}Mn_{0.3}O_9$. Since the presence of perovskite *A*-site cations with $6s^2$ lone pairs such as Bi^{3+} and Pb^{2+} strongly favors a highly distorted structure and induces an increase in T_c [8,25], the substitution of La^{3+} for Pb^{2+} on the *A*-site reduces the concentration of *A*-site lone pair cations, leading to a smaller degree of distortion and hence a lower Curie temperature. The decrease of T_c is also consistent with the larger Goldschmidt tolerance factor (t) of the perovskite block of $Pb_{0.4}Bi_{2.1}La_{0.5}Nb_{1.7}Mn_{0.3}O_9$ (0.940) compared to $PbBi_2Nb_2O_9$ (0.932) [6].

The dielectric peak exhibits a strong frequency dependence with

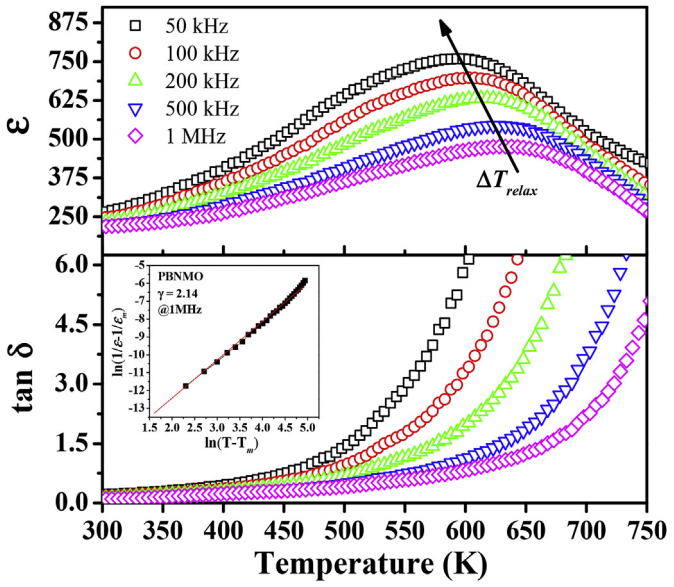

Fig. 4. Temperature dependence of dielectric constant (ϵ) and loss (tan δ) of $Pb_{0.4}Bi_{2.1}La_{0.5}Nb_{1.7}Mn_{0.3}O_9$. The inset shows a modified Curie-Weiss fitted line to quantify relaxor ferroelectric behavior.

a temperature relaxation $\Delta(T_{m(1MHz)} - T_{m(50kHz)})$ of around 40 K, which confirms pronounced relaxor-ferroelectric behavior [26]. This behavior can also be described by the degree of diffuseness (γ) using a modified Curie-Weiss law [15]. The inset of Fig. 4 shows a linear fit to a plot of $ln(1/\epsilon_r - 1/\epsilon_m)$ versus $ln(T\text{-}T_m)$ at 1 MHz, where the value of $\gamma = 1$ represents normal ferroelectric behavior and $\gamma = 2$ is typical for relaxor-ferroelectric. The fitted value of γ is 2.14. This relaxor behavior is strongly correlated with the compositional disorder on all the cation sites.

Room temperature *P-E* hysteresis loops measured at 40 Hz under various electric field ranges are shown in Fig. 5. At 60 kV/cm, the hysteresis loop is unsaturated, implying that higher electric fields are needed to align all the domains. At the highest applied

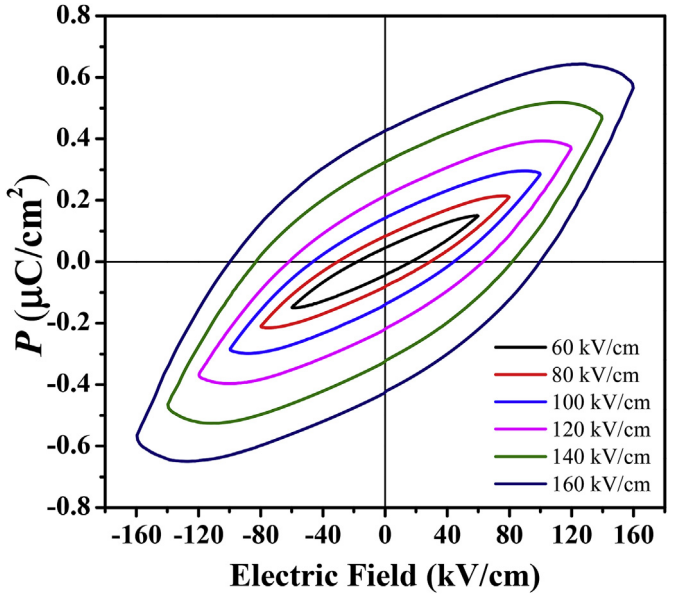

Fig. 5. *P-E* hysteresis loops of $Pb_{0.4}Bi_{2.1}La_{0.5}Nb_{1.7}Mn_{0.3}O_9$ measured at room temperature and 40 Hz frequency.

electric field of 160 kV/cm before electrical breakdown occurred, the loop is still unsaturated, which is likely due to leakage currents [11,27]. The substitution of Mn^{3+} for Nb^{5+} in $Pb_{0.4}Bi_{2.1}La_{0.5}Nb_{1.7}Mn_{0.3}O_9$ increases the electron concentration and thus the electrical conductivity, hence the high leakage current and significant dielectric loss [23]. Although leaky, both the remnant polarization (P_r) and saturated polarization (P_s) increase with electric field in non-linear fashion. This behavior reflects domain wall motion associated with ferroelectricity [28]. The remnant polarization (P_r) and the coercive field (E_c) are 0.43 μC/cm^2 and 99.7 kV/cm, respectively, under the maximum electric field of 160 kV/cm. The ferroelectric polarization in this sample is correlated with off-center displacement of the *B*-site cation in the *a*-direction, according to $A2_1am$ symmetry. It has previously been argued that octahedral tilting, as shown in Fig. 2(b), can further enhance the shift of this cation along the *a*-axis [9].

To investigate the magnetic properties of $Pb_{0.4}Bi_{2.1}La_{0.5}Nb_{1.7}Mn_{0.3}O_9$, we performed magnetic susceptibility versus temperature and magnetization versus applied field measurements. Fig. 6(a) shows the magnetic susceptibility and inverse susceptibility in zero-field-cooled (ZFC) mode measured on warming in an applied magnetic field of 1 T. The ZFC susceptibility (χ) curve indicates paramagnetic-like behavior with no evidence of long-range magnetic ordering, as evidenced by the monotonous decrease of χ with increasing temperature. However, a Curie-Weiss fit to the linear region of the $1/\chi$–T curve above 100 K yields a positive Curie-Weiss temperature (θ_{CW}) of 33.44 K, indicating the predominance of ferromagnetic interactions. To verify the existence of ferromagnetic interactions, the ZFC susceptibility was measured in a lower applied field of 100 Oe as shown in Fig. 6(b). An obvious ferromagnetic-paramagnetic transition at $T_c = 33.5$ K is now observed, where T_c is obtained from the maximum of the ($d\chi$/dT) curve; this temperature is consistent with the fitted θ_{CW}. This is also close to the value of T_c (21.5 K) for the Mn-doped Aurivillius phase $PbBi_4Ti_4O_{15}$, where 15% of Ti^{4+} on the *B*-site was replaced by Mn [12].

The effective moment (μ_{eff}) per Mn ion calculated from the Curie-Weiss fit is 4.38 μ_B. The spin-only values of μ_{eff} for high-spin Mn^{3+} and Mn^{4+} are 4.90 μ_B and 3.87 μ_B, respectively [29,30]. Thus, the sample likely contains approximately equal proportions of Mn^{3+} and Mn^{4+}. The mixed-valent Mn^{3+}/Mn^{4+} may enable double-exchange to take place, giving rise to the weakly ferromagnetic behavior. The magnetic ordering will be short-range in nature because only 15% of the *B*-site is occupied by Mn, far below the percolation threshold. Furthermore, strong ferromagnetic behavior has mainly been observed in Aurivillius phases with a thicker perovskite block than our two-layer $Pb_{0.4}Bi_{2.1}La_{0.5}Nb_{1.7}Mn_{0.3}O_9$, such as the four-layered structure, and can be enhanced by combining two magnetic cations in a 1:1 ratio [31,32]. We speculate that the double exchange pathway may be in the *ab*-plane via Mn(1)-O(4)-Mn(1) and Mn(1)-O(5)-Mn(1), which are depicted in Fig. 2(c). These exchange interactions might occur in locally Mn-rich areas, the presence of which was previously suggested by the vibrational mode at 756 cm^{-1} in Raman spectra [17]. A preference for local ordering of the magnetic cation was also observed previously in $SrBi_2Nb_{2-x}Fe_xO_9$, where (Fe–O–Fe) super-exchange interactions are of relevance [33]. Such local ordering is also evidenced by the high dielectric loss and leakage current in $Pb_{0.4}Bi_{2.1}La_{0.5}Nb_{1.7}Mn_{0.3}O_9$ [23], which are attributed to double exchange involving Mn^{3+}-O-Mn^{4+}.

Fig. 7 shows magnetization versus applied field $M(H)$ measurements for $Pb_{0.4}Bi_{2.1}La_{0.5}Nb_{1.7}Mn_{0.3}O_9$ at 5 K and 150 K. The magnetization does not reach saturation in the applied field range −5 T to 5 T. The M(H) curve at 5 K adopts the typical *S*-shaped, narrow hysteresis loop of a weak ferromagnetic, where M_r and H_c

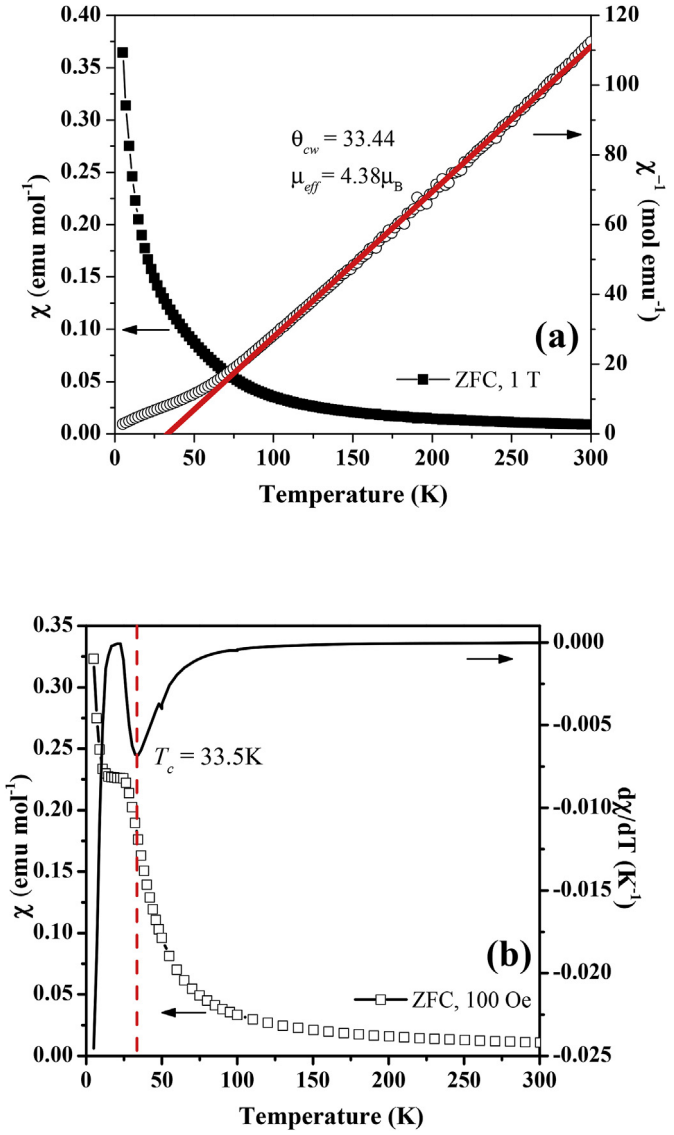

Fig. 6. **(a)** Temperature dependence of ZFC magnetic susceptibility (χ) and inverse magnetic susceptibility (1/χ) measured in an applied field of 1 T. The red line is a linear fit to the experimental data using the Curie-Weiss law. **(b)** ZFC magnetic susceptibility (χ) and its derivative (dχ/dT) measured in an applied field of 100 Oe. (For interpretation of the references to colour in this figure legend, the reader is referred to the Web version of this article.)

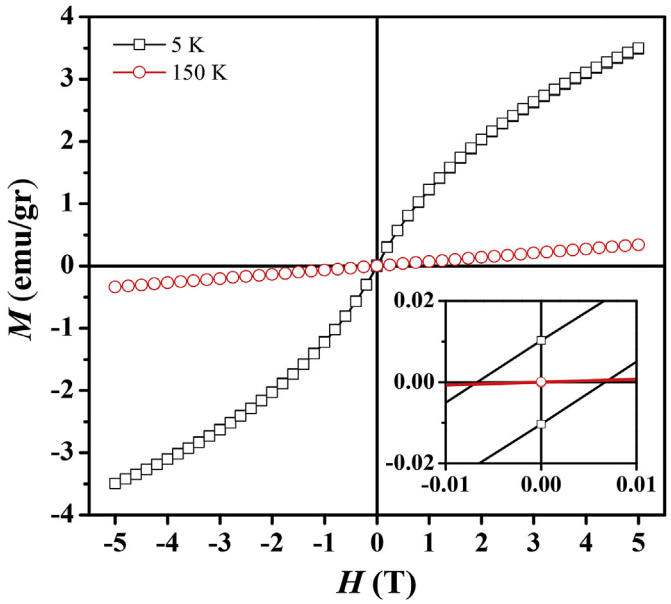

Fig. 7. Magnetization versus applied field for $Pb_{0.4}Bi_{2.1}La_{0.5}Nb_{1.7}Mn_{0.3}O_9$ measured at 5 K and 150 K.

are estimated to be 0.01 emu/g and 67 Oe. At 150 K, where the sample is far above the T_c of 33 K, linear behavior is observed with no loop opening, as typical for paramagnetic behavior.

4. Conclusion

A single-phase sample of the Aurivillius material $Pb_{0.4}Bi_{2.1}La_{0.5}Nb_{1.7}Mn_{0.3}O_9$ has been synthesized by a molten salt method using K_2SO_4/Na_2SO_4. Rietveld refinement using neutron diffraction data suggested considerable cation disorder, where La atoms partially occupy the perovskite *A*-site, Pb/Bi atoms occupy both the perovskite A-site and bismuth oxide block, and Nb/Mn occupy the perovskite *B*-site. The dielectric constant exhibits a broad frequency-dependent peak indicating a ferroelectric transition temperature (T_c) of 600–640 K, which is typical for a relaxor ferroelectric. The disorder associated with the simultaneous substitution of La^{3+} and Mn^{3+} in $PbBi_2Nb_2O_9$ is likely responsible for the relaxor ferroelectric behavior. Ferroelectric *P-E* loops remain unsaturated in applied electric fields up to 160 kV/cm and a maximum P_r of 0.43 μC/cm^2 was obtained. Magnetic susceptibility measurements indicated that manganese is present in the mixed-valence state of Mn^{3+}/Mn^{4+}. A positive Curie-Weiss temperature and a peak in the susceptibility at 33 K indicate the presence of ferromagnetic interactions and short-range order which are assumed to arise from double-exchange involving Mn^{3+}-O-Mn^{4+} bonds in the BO_6 octahedra. In conclusion, the Aurivillius compound $Pb_{0.4}Bi_{2.1}La_{0.5}Nb_{1.7}Mn_{0.3}O_9$ exhibits the coexistence of both ferroelectric and ferromagnetic properties facilitating applications in memory storage devices.

Declaration of competing interest

The authors declare that they have no known competing financial interests or personal relationships that could have appeared to influence the work reported in this paper.

Acknowledgments

This work was supported by the Ministry of Research, Technology and Higher Education (RISTEKDIKTI) of the Republic of Indonesia through a PMDSU Scholarship [Grant number 050/SP2H/LT/DRPM/2018] and a PKPI-PMDSU Scholarship [Grant number 1406.29/D3/PG/2018].

References

[1] A.J.C. Buurma, G.R. Blake, T.T.M. Palstra, Multiferroic Materials : Physics and Properties, Elsevier Ltd., 2016, https://doi.org/10.1016/B978-0-12-803581-8.09245-6.
[2] S.N. Achary, O.D. Jayakumar, A.K. Tyagi, Multiferroic Materials, Elsevier Inc., 2012, https://doi.org/10.1016/B978-0-12-385142-0.00004-0.
[3] S. Ivanov, Multiferroic Complex Metal Oxides : Main Features of Preparation , Structure , and Properties, Elsevier Inc., 2012, https://doi.org/10.1016/B978-0-44-453681-5.00007-8.
[4] B. Aurivillius, Mixed bismuth oxides with layer lattice I, Ark. Kemi. 1 54 (1949) 463–480.
[5] J.F. Scott, Ferroelectric Memories, first ed., Springer-Verlag Berlin Heidelberg, New York, 2000 https://doi.org/10.1007/978-3-662-04307-3.

[6] D.Y. Suárez, I.M. Reaney, W.E. Lee, Relation between tolerance factor and Tc in Aurivillius compounds, J. Mater. Res. 16 (2001) 3139–3149, https://doi.org/10.1557/JMR.2001.0433.
[7] E.V. Ramana, M.P.F. Graça, M.A. Valente, T.B. Sankaram, Improved ferroelectric and pyroelectric properties of Pb-doped $SrBi_4Ti_4O_{15}$ ceramics for high temperature applications, J. Alloy. Comp. 583 (2014) 198–205, https://doi.org/10.1016/j.jallcom.2013.08.181.
[8] Ismunandar, B.A. Hunter, B.J. Kennedy, Cation disorder in the ferroelectric Aurivillius phase $PbBi_2Nb_2O_9$: an anamolous dispersion X-ray diffraction study, Solid State Ion. 112 (1998) 281–289, https://doi.org/10.1016/S0167-2738(98)00222-7.
[9] A.B. Missyul, I.A. Zvereva, T.T.M. Palstra, A.I. Kurbakov, Double-layered Aurivillius-type ferroelectrics with magnetic moments, Mater. Res. Bull. 45 (2010) 546–550, https://doi.org/10.1016/j.materresbull.2010.02.002.
[10] C.C. Chou, C.L. Huang, S. Mukherjee, Q.Y. Chen, H. Sakurai, A.A. Belik, E.T. Muromachi, H.D. Yang, Multiple magnetic transitions in multiferroic $BiMnO_3$, Phys. Rev. B (2009) 184426, https://doi.org/10.1103/PhysRevB.80.184426.
[11] S. Liu, S. Yan, H. Luo, L. Yao, Z. Hu, S. Huang, L. Deng, Enhanced magnetoelectric coupling in La-modified $Bi_5Co_{0.5}Fe_{0.5}Ti_3O_{15}$ multiferroic ceramics, J. Mater. Sci. 53 (2018) 1014–1023, https://doi.org/10.1007/s10853-017-1604-6.
[12] Zulhadjri, B. Prijamboedi, A.A. Nugroho, N. Mufti, A. Fajar, T.T.M. Palstra, Ismunandar, Aurivillius phases of $PbBi_4Ti_4O_{15}$ doped with Mn^{3+} synthesized by molten salt technique: structure, dielectric, and magnetic properties, J. Solid State Chem. 184 (2011) 1318–1323, https://doi.org/10.1016/j.jssc.2011.03.044.
[13] P. Fang, P. Liu, Z. Xi, W. Long, X. Li, Structure and electrical properties of new Aurivillius oxides $(K_{0.1}6Na_{0.84})_{0.5}Bi_{4.5}Ti_4O_{15}$ with manganese modification, J. Alloy. Comp. 595 (2014) 148–152, https://doi.org/10.1016/j.jallcom.2014.01.152.
[14] Z.P. Cao, C.M. Wang, K. Lau, Q. Wang, Q.W. Fu, H.H. Tian, D.F. Yin, Large enhancement of piezoelectric properties in Mn-modified $SrBi_4Ti_4O_{15}$ and its thermal stabilities at elevated temperatures, Ceram. Int. 42 (2016) 11619–11625, https://doi.org/10.1016/j.ceramint.2016.04.061.
[15] M. Roy, I. Bala, S.K. Barbar, S. Jangid, P. Dave, Synthesis, structural and electrical properties of La and Nb modified $Bi_4Ti_3O_{12}$ ferroelectric ceramics, J. Phys. Chem. Solids 72 (2011) 1347–1353, https://doi.org/10.1016/j.jpcs.2011.08.007.
[16] A. Khokhar, P.K. Goyal, O.P. Thakur, A.K. Shukla, K. Sreenivas, Influence of lanthanum distribution on dielectric and ferroelectric properties of $BaBi_{4-x}La_xTi_4O_{15}$ ceramics, Mater. Chem. Phys. 152 (2015) 13–25, https://doi.org/10.1016/j.matchemphys.2014.11.074.
[17] T.P. Wendari, S. Arief, N. Mufti, V. Suendo, A. Prasetyo, J. Baas, G.R. Blake, Zulhadjri, Synthesis, structural analysis and dielectric properties of the double-layer Aurivillius compound $Pb_{1-2x}Bi_{1.5+2x}La_{0.5}Nb_{2-x}Mn_xO_9$, Ceram. Int. 45 (2019) 17276–17282, https://doi.org/10.1016/j.ceramint.2019.05.285.
[18] B.A. Hunter, C.J. Howard, A Computer Program for Rietveld Analysis of X-Ray and Neutron Powder Diffraction Patterns, Lucas Heights Research Laboratories, NSW, Australia, 2000, pp. 1–27.
[19] V. Srikanth, H. Idink, W.B. White, E.C. Subbarao, H. Rajagopal, A. Sequeira, Cation disorder in ferroelectric $PbBi_2Nb_2O_9$, Acta Crystallogr. 52 (1996) 432–439, https://doi.org/10.1107/S0108768195015072.
[20] T. Rentschler, M. Karus, A. Wellm, A. Reller, Synthesis and characterization of the Aurivillius phases $Bi_{2-x}Pb_xSr_{1-x}Nd_xNb_2O_9$, Solid State Ion. 90 (1996) 49–55.
[21] B.J. Kennedy, B.A. Hunter, Cation disorder in Pb-doped $SrBi_2Nb_2O_9$, Chem. Mater. 13 (2006) 4612–4617.
[22] J. Xiao, H. Zhang, Y. Xue, Z. Lu, X. Chen, P. Su, F. Yang, X. Zeng, The influence of Ni-doping concentration on multiferroic behaviors in $Bi_4NdTi_3FeO_{15}$ ceramics, Ceram. Int. 41 (2015) 1087–1092, https://doi.org/10.1016/j.ceramint.2014.09.033.
[23] P. Nayak, T. Badapanda, A.K. Singh, S. Panigrahi, An approach for correlating the structural and electrical properties of Zr^{4+}-modified $SrBi_4Ti_4O_{15}$/SBT ceramic, RSC Adv. 7 (2017) 16319–16331, https://doi.org/10.1039/c7ra00366h.
[24] H. Du, Y. Li, H. Li, X. Shi, C. Liu, Relaxor behavior of bismuth layer-structured ferroelectric ceramic with m = 2, Solid State Commun. 148 (2008) 357–360, https://doi.org/10.1016/j.ssc.2008.05.017.
[25] S.M. Blake, M.J. Falconer, M. Mccreedy, P. Lightfoot, Cation disorder in ferroelectric Aurivillius phases of the type $Bi_2ANb_2O_9$ (A=Ba, Sr, Ca), J. Mater. Chem. 7 (1997) 1609–1613, https://doi.org/10.1039/A608059F.
[26] V.V. Shvartsman, D.C. Lupascu, Lead-free relaxor ferroelectrics, J. Am. Ceram. Soc. 95 (2012) 1–26, https://doi.org/10.1111/j.1551-2916.2011.04952.x.
[27] Y. Shi, Y. Pu, J. Li, R. Shi, W. Wang, Q. Zhang, L. Guo, Structure , dielectric and multiferroic properties of three-layered aurivillius $SrBi_3Nb_2FeO_{12}$, Ceram. Int. 45 (2019) 9283–9287, https://doi.org/10.1016/j.ceramint.2019.01.129.
[28] M.R. Dolgos, U. Adem, A. Manjon-sanz, X. Wan, T.P. Comyn, T. Stevenson, J. Bennett, A.J. Bell, T.T. Tran, P.S. Halasyamani, J.B. Claridge, M.J. Rosseinsky, Perovskite B-Site compositional control of [110]$_p$ polar displacement coupling in an ambient-pressure-stable bismuth-based ferroelectric, Angew. Chem. 124 (2012) 10928–10933, https://doi.org/10.1002/ange.201203884.
[29] C.A. López, M.E. Saleta, J.C. Pedregosa, R.D. Sánchez, J.A. Alonso, M.T. Fernández-Díaz, Cationic disorder and Mn^{3+}/Mn^{4+} charge ordering in the B' and B'' sites of $Ca_3Mn_2NbO_9$ perovskite : a comparison with $Ca_3Mn_2WO_9$, J. Solid State Chem. 210 (2014) 1–9, https://doi.org/10.1016/j.jssc.2013.10.039.
[30] K. Nakade, K. Hirota, M. Kato, H. Taguchi, Effect of the Mn^{3+} ion on electrical and magnetic properties of orthorhombic perovskite-type $Ca(Mn_{1-x}Ti_x)O_{3-\delta}$, Mater. Res. Bull. 42 (2007) 1069–1076, https://doi.org/10.1016/j.materresbull.2006.09.013.
[31] Z. Yu, X. Meng, Z. Zheng, Y. Lu, H. Chen, C. Huang, H. Sun, K. Liang, Z. Ma, Y. Qi, T. Zhang, Room temperature multiferroic properties of rare-earth-substituted Aurivillius phase $Bi_5Ti_3Fe_{0.7}Co_{0.3}O_{15}$ ceramics, Mater. Res. Bull. 115 (2019) 235–241, https://doi.org/10.1016/j.materresbull.2019.04.002.
[32] Y. Shu, Q. Ma, Z. Ding, L. Cao, X. Chen, F. Yang, X. Zeng, Multiferroic behaviors of Co-doped $Bi_4NdTi_3FeO_{15}$ ceramics, Phys. Lett. A 383 (2019) 911–914, https://doi.org/10.1016/j.physleta.2018.12.031.
[33] Y. Shi, Y. Pu, Q. Zhang, J. Li, L. Guo, Dielectric and multiferroic properties of two-layered $SrBi_2Nb_{2-x}Fe_xO_9$Aurivillius compounds, Ceram. Int. 44 (2018) S61–S64, https://doi.org/10.1016/j.ceramint.2018.08.251.